Osmotically Induced Shape Changes of Large Unilamellar Vesicles Measured by Dynamic Light Scattering

Jeremy Pencer, Gisèle F. White, and F. Ross Hallett

Biophysics Interdepartmental Group and Department of Physics, University of Guelph, Guelph, Ontario N1G 2W1, Canada

ABSTRACT Static and dynamic light scattering measurements have been used to characterize the size, size distribution, and shape of extruded vesicles under isotonic conditions. Dynamic light scattering was then used to characterize osmotically induced shape changes by monitoring changes in the hydrodynamic radius (R_h) of large unilamellar vesicles (LUVs). These changes are compared to those predicted for several shapes that appear in trajectories through the phase diagram of the area difference elasticity (ADE) model (Jarić et al. 1995. *Phys. Rev. E.* 52:6623–6634). Measurements were performed on dioleoylphosphatidylcholine (DOPC) vesicles using two membrane-impermeant osmolytes (NaCl and sucrose) and a membrane-permeant osmolyte (urea). For all conditions, we were able to produce low-polydispersity, nearly spherical vesicles, which are essential for resolving well-defined volume changes and consequent shape changes. Hyper-osmotic dilutions of DOPC vesicles in urea produced no change in R_h, whereas similar dilutions in NaCl or sucrose caused reductions in vesicle volume resulting in observable changes to R_h. Under conditions similar to those of this study, the ADE model predicts an evolution from spherical to prolate then oblate shapes on increasing volume reduction of LUVs. However, we found that DOPC vesicles became oblate at all applied volume reductions.

INTRODUCTION

Unilamellar vesicles have been the subject of a great deal of experimental study due to their importance as drug delivery systems (Gregoriadis, 1995) and value as model systems for more complex biological membranes (Sackmann, 1995). Membrane curvature and elasticity have been implicated as important factors determining the stability and function of both biological and artificial membranes (Sackmann, 1995; Wood, 1999). Recently, there have been several demonstrations of the importance of membrane curvature in biological processes, such as the refolding kinetics of bacteriorhodopsin (Booth, 1997), and modulation of the activity of Phospholipase A_2 (Burack, 1997). Consequently, studies of membrane curvature play an important role in the elucidation of membrane-related biological processes and the development of liposome-based technologies.

Since the initial implication of the role of bending energy in determining the shape of biological membranes (Helfrich, 1973), much effort has been spent in the construction and study of theoretical models to predict observed shapes and shape changes of membrane systems (Helfrich, 1973; Svetina and Žekš, 1983; Seifert et al., 1991; Miao et al., 1994; Jarić et al., 1995). Two models, the spontaneous curvature (SC) model (Helfrich, 1973) and the bilayer coupling (BC) model (Svetina and Žekš, 1983), have received historically a great deal of attention. The SC model is defined in terms of the energy cost associated with the curvature at a point on the membrane surface. The BC model, in contrast, is defined by the energy cost associated with the curvature-induced area difference between the inner and outer monolayers of the membrane. Because these models depend on different vesicle properties, their predictions for the shape behavior of vesicles are qualitatively very different (Seifert et al., 1991). In general, neither the SC nor BC models alone are sufficient to describe membrane curvature (Miao et al., 1994). More recently, the area difference elasticity (ADE) model was developed, which combines features of both the SC and BC models, and represents a more complete model of membrane-bending energy (Miao et al., 1994; Jarić et al., 1995).

To date, most experimental studies of vesicle shape have been performed on giant unilamellar vesicles (GUVs) with sizes ranging from 1 to 10 μm in radius (Döbereiner, 2000, and references therein). Typical studies of GUVs are based on optical microscopy measurements on single vesicles. Bending elasticities of GUVs have been measured using contour analysis of fluctuations (Döbereiner et al., 1997) and using pipette aspiration measurements (Rawicz et al., 2000). Microscopy measurements have been combined with fluorescence measurements to correlate shape changes with lateral phase separation within the membrane (Bagatolli and Gratton, 1999). Attempts have been made to provide a rigorous comparison between experimental results and predictions from the ADE model (Miao et al., 1994; Döbereiner et al., 1997). Results from these studies have demonstrated that GUV shape behavior is well described by the ADE model.

There have also been studies on small unilamellar vesicles (SUVs) ~15-nm radius and large unilamellar vesicles (LUVs) ~50-nm radius. These studies fall into two classes: measurements of shapes and shape changes (Talmon et al., 1990; Hallett et al., 1991a; Lerebours et al., 1993; Mui et al., 1993, 1995; White et al., 1996, 2000; Edwards et al., 1997; Beney et al., 1998; Korgel et al., 1998; Jin et al., 1999) and

Received for publication 22 January 2001 and in final form 31 July 2001.

Address reprint requests to F. Ross Hallett, Univ. of Guelph, Dept. of Physics, Guelph, Ont. N1G 2W1, Canada. Tel.: 519-824-4120x3989; Fax: 519-836-9967; E-mail: frh@physics.uoguelph.ca.

0006-3495/01/11/2716/13 $2.00

measurements of shape fluctuations (Xu and Döbereiner, 1999; Brocca et al., 2000). It is commonly accepted that vesicles prepared by extrusion in the presence of buffer or impermeable solutes are not spherical (Mui et al., 1993; Jin et al., 1999). In fact, a variety of studies have provided evidence that vesicles extruded in the presence of solute or buffer can be spherical (Edwards et al., 1997; Korgel et al., 1998), prolate (Edwards et al., 1997; Jin et al., 1999), or exhibit a variety of morphologies (Talmon et al., 1990; Mui et al., 1993, 1995; Agirre et al., 2000). In the case of nonspherical vesicles, it has been shown that exposure to hypo-osmotic gradients results in a change to a spherical shape (Mui et al., 1993; Jin et al., 1999). Exposure of spherical vesicles to hyper-osmotic shifts results in changes to vesicle shape or apparent size (Lerebours et al., 1993; White et al., 1996, 2000; Beney et al., 1998). However, the nature of these shape changes appears to depend on the initial vesicle size, composition, or initial shape state. There have been attempts in some of these studies (Mui et al., 1995; Xu and Döbereiner, 1999) to make comparisons with predictions of the ADE model. However, accurate comparisons were complicated by a polydispersity in vesicle shape in the case of Mui et al. (1995) or low sampling size in the case of Xu and Döbereiner (1999).

In this paper, we investigate osmotic effects on vesicle shape using a system for which measurements are not complicated by factors such as initial shape polydispersity or complex lipid composition. In particular, we will follow the methods used by Beney et al. (1998). We create shape changes by diluting vesicles into hyper-osmotic media. Osmotically induced volume changes result in vesicle shape changes because of the relative incompressibility of the membrane bilayer. By defining the state of the vesicles prior to osmotic changes, we expect to be able to guide the vesicles along specific trajectories in the ADE phase diagram (Wortis et al., 1997). Static (SLS) and dynamic (DLS) light scattering are used to characterize the initial state of extruded vesicles, prior to hyper-osmotic dilution. DLS is then used to measure osmotically induced changes to the vesicle diffusion coefficients and corresponding hydrodynamic radii. We then compare relative changes in hydrodynamic radii to those predicted, based on induced volume changes for several axisymmetric shapes appearing in the ADE phase diagram.

MATERIALS AND METHODS

Preparation of extruded vesicles

1,2-dioleoyl-sn-glycero-3-phosphocholine (DOPC) and 1-stearoyl-2-oleoyl-*sn*-glycero-3-phosphocholine (SOPC) were purchased from Avanti Polar Lipids, Inc. (Birmingham, AL) and used without further purification. All other chemicals were reagent grade. Extruded vesicles were prepared as described previously (White et al., 1996). Lipids were shipped from the supplier solubilized in methylene chloride and stored at −40°C. Lipid was transferred to round-bottom flasks and methylene chloride was removed from solubilized lipid by a two-stage process, rotary evaporation followed by vaccuum pumping. The lipid film was then dissolved under argon in MOPS buffer (20 mM MOPS, 0.5 mM EDTA, pH 7.4) plus the appropriate solute (NaCl, sucrose or urea). The dispersion was freeze–thawed ten times, by alternating immersion of the round-bottom flask in liquid nitrogen and warm water at 37°C. The lipid dispersion was then extruded using a hand-held extrusion device (MacDonald et al., 1991). To investigate effects of the number of extrusion steps on vesicle shape and polydispersity, four samples were prepared with successively greater numbers of extrusions. The first sample was extruded seven times through a 200-nm-diameter pore polycarbonate filter; the second was made by extruding the extrudate of the first sample seven times through a 100-nm-diameter pore filter; the third was made by seven further extrusions through a 100-nm-diameter pore filter; the fourth was made by an additional fifteen extrusions through a 100-nm-diameter pore filter. The polycarbonate filters were replaced between each preparation. Vesicles used in the hyper-osmotic dilution experiments were extruded using the maximum number of extrusion steps described above. Vesicles used for static and dynamic light scattering were diluted from an initial concentration of 50 mg/ml under isotonic conditions to a final concentration of 0.05 mg/ml in the appropriate (iso or hyper-tonic) buffer solution.

Dynamic light scattering

DLS measurements were performed using a diode-pumped, frequency-doubled Nd:YAG laser (λ of 532 nm) and a Brookhaven digital autocorrelator and software (BI-9000AT and 9kDLSW control program, BIC, Holtsville, NY). All measurements were taken at a scattering angle, θ, of 90°. DLS measures the autocorrelation function $g^1(\tau)$, which is related to the size distribution of vesicles in solution by (Johnson and Gabriel, 1994)

$$g^{(1)}(\tau) = \int_0^\infty m_\Gamma^2 \, P(q, \Gamma) G(\Gamma) e^{-\Gamma\tau} \, d\Gamma, \qquad (1)$$

where $G(\Gamma)$ is the normalized number distribution function for the decay constants Γ, m_Γ is the particle mass, $P(q, \Gamma)$ is the particle scattering factor (as discussed in the following section), the decay constant $\Gamma = q^2 D_T$, the scattering vector $q = (4\pi n/\lambda)\sin(\theta/2)$, θ is the angle between the incident and scattered beam, n is the refractive index of the medium, and D_T is the translational diffusion coefficient. D_T is related to the hydrodynamic radius, R_h, by (Johnson and Gabriel, 1994)

$$D_T = \frac{k_B T}{6\pi\eta R_h}, \qquad (2)$$

where k_B is Boltzmann's constant, T is the temperature, and η is the viscosity of the medium. For spherical vesicles, R_h is equal to the outer radius (which may also include a surface layer of bound water or solute). However, for nonspherical vesicles, R_h will depend not only on the vesicle size, but also on the vesicle shape. The relationship between R_h and vesicle shape is calculated for several shapes in Appendix A. Changes in vesicle size or shape will result in corresponding changes the measured hydrodynamic radius.

For the hyper-osmotic shift experiments, the diffusion coefficients of vesicles were determined by fitting data using a third-order cumulant expansion given by

$$\ln(g^1(\tau)) = -q^2\langle D_T\rangle\tau + \frac{\mu_2}{2!} q^4\tau^2 + O(\tau^3), \qquad (3)$$

where $\langle D_T\rangle$ is the average translational diffusion coefficient, and the relative variance of $\langle D_T\rangle$ is given by $\mu_2/\langle D_T\rangle^2$, which is often quoted as a measure of the polydispersity, Δ^2 (Johnson and Gabriel, 1994). The average hydrodynamic radius determined by cumulants, which we will denote

as $\langle R_h \rangle$, is calculated from $\langle D_T \rangle$ using Eq. 2 and is related to the vesicle number distribution $G(R_a)$ by

$$\langle R_h \rangle \equiv \frac{kT}{6\pi\eta} \langle D_T \rangle^{-1} = \left(\int_0^\infty R_h^{-1} P(q, R_h) m_{Rh}^2 G(R_h)\, dR_h \right)^{-1} \times \left(\int_0^\infty P(q, R) G(R_h) m_{Rh}^2\, dR_h \right), \quad (4)$$

where $G(R_h)\, dR_h = G(\Gamma)\, d\Gamma$ (Hallett et al., 1991b) and m_{Rh} is the mass of vesicles with hydrodynamic radius, R_h. The corresponding polydispersity is related to the vesicle number distribution $G(R_h)$ by

$$\Delta^2 = \left[\left(\int_0^\infty R_h^{-2} P(q, R_h) m_{Rh}^2 G(R_h)\, dR_h \right)^{-1} \times \left(\int_0^\infty P(q, R_h) m_{Rh}^2 G(R_h)\, dR_h \right) - \langle R_h \rangle^2 \right] \Big/ \langle R_h \rangle^2. \quad (5)$$

Later in this paper, we will refer to the intensity-weighted size distribution, which we define as $G'(R) = P(q, R) m_R^2 G(R)$. For sufficiently small particles, or small q, $P(q, R) \approx 1$, $G'(R) \approx m_R^2 G(R)$, and cumulants analysis gives the z (mass squared) average hydrodynamic radius and polydispersity (Koppel, 1972). However, for extruded vesicles (typically 30 nm or greater in radius), the particle form factor makes a significant contribution to the actual values of $\langle R_h \rangle$ and Δ^2 as determined by cumulants. Unless otherwise stated, DLS results are averaged over ten consecutive measurements, and error bars correspond to one standard deviation.

Intensity-weighted distributions of hydrodynamic radii for samples under isotonic conditions were determined from DLS data using a discrete Laplace inversion routine as previously described in earlier works (Hallett et al., 1989, 1991b). These measurements give the relative intensity weightings of vesicles as a function of hydrodynamic radius $G'(R_h)$. From these intensity-weighted distributions $G'(R_h)$, vesicle number distributions are calculated as described in the Theory section and Appendix B. For isotonic samples, results of full inversions of DLS data are averaged over three runs of at least 2 h each.

Static light scattering

SLS measurements were performed using a Malvern 4700 Series Spectrometer with a Siemens Helium-Neon laser (λ of 632.8 nm, Malvern Instruments, Worchestershire, UK). Measurements were taken for θ ranging from 30° to 140°. Calibration of the instrument was performed using reagent-grade toluene. SLS data gives the time-averaged scattered intensity from dilute particles in suspension as a function of scattering vector q, given by

$$\frac{I(q)}{I_0} \propto k^4 N M^2 \left(\frac{m^2 - 1}{m^2 + 2} \right)^2 P(q), \quad (6)$$

where $k = 2\pi n_0/\lambda$, $m = n_1/n_0$, n_0 is the medium refractive index, n_1 is the refractive index of the particles, λ is the laser wavelength, N is the number concentration of particles, M is the particle mass, and the particle scattering factor $P(q)$ depends on particle size and shape.

At low values of q, where, $qR_g < 1$, we can approximate the scattering factor $P(q)$ by a shape-independent function, the Guinier approximation, given by (Guinier, 1994)

$$P(q) \approx \exp\left(\frac{-q^2 R g^2}{3} \right), \quad (7)$$

where R_g is the polarizability-weighted radius of gyration. By fitting the low q range of the SLS data, we can apply the Guinier approximation to determine the radius of gyration. For polydisperse particles, the Guinier approximation gives the z average of R_g^2, given by

$$\langle R_g^2 \rangle = \frac{\int_0^\infty R_g^2 m_R^2 G(R)\, dR}{\int_0^\infty m_R^2 G(R)\, dR}. \quad (8)$$

We denote the experimentally determined radius of gyration as $\langle R_g \rangle \equiv \langle R_g^2 \rangle^{1/2}$.

We have also simulated SLS data using Rayleigh–Gans–Debye (RGD) scattering factors for spherical and prolate vesicles. The normalized RGD scattering factor for spherical vesicles is given by

$$P(q) = \left[\frac{3}{u^3 - \nu^3} \right]^2 \left[u^3 \frac{j_1(qu)}{qu} - \nu^3 \frac{j_1(q\nu)}{q\nu} \right]^2, \quad (9)$$

where, $u = R + t/2$, $\nu = R - t/2$, R is the radius, t is the membrane thickness, and $j_1(x)$ is the first-order spherical Bessel function given by

$$j_1(x) = \frac{\sin x}{x^2} - \frac{\cos x}{x}. \quad (10)$$

The RGD scattering factor for prolate vesicles is given by

$$P(q) = \left[\frac{3}{u - \nu} \right]^2 \int_0^1 \left[u \frac{j_1(qU)}{qU} - \nu \frac{j_1(qV)}{qV} \right]^2 dx, \quad (11)$$

where

$$U = \sqrt{a_0^2 x^2 + b_0^2 (1 - x^2)},$$

$$V = \sqrt{a_i^2 x^2 + b_i^2 (1 - x^2)},$$

$$u = a_0 b_0^2, \quad \nu = a_i b_i^2, \quad a_0 = a + t/2,$$

$$b_0 = b + t/2, \quad a_i = a - t/2, \quad b_i = b - t/2,$$

t is the membrane thickness, a is the length of the vesicle long axis (or symmetry axis), and b is the length of the vesicle short axis.

THEORY

Predictions of the ADE model for vesicle shape changes

The ADE model describes the curvature energy of a membrane as the sum of two terms, one that depends on the curvature at any point on the membrane surface, and a second that depends on the curvature-induced area differ-

ence between the inner and outer monolayers. This model can be used to determine minimum energy shapes of vesicles as a function of parameters such as the enclosed volume V. The total curvature energy of a membrane as determined by the ADE model is given by the surface integral (Jarić et al., 1995),

$$W = \frac{k_c}{2}\left[\oint dA\left(\frac{1}{R_1}+\frac{1}{R_2}-C_0\right)^2 + \frac{\pi\alpha}{AD^2}(\Delta A-\Delta A_0)^2\right], \tag{12}$$

where k_c is the local bending modulus, R_1 and R_2 are the principal radii of curvature at any point on the membrane surface, C_0 is the spontaneous curvature, D is the membrane thickness, A is the average membrane area, ΔA is the difference between the areas of the inner and outer monolayers, ΔA_0 is the relaxed area difference, and α is the ratio of the local, k_c, to nonlocal, k_t, bending moduli. The parameter α provides a measure of the relative contributions of the spontaneous curvature and relaxed area difference to the bending energy and is typically of order 1 for phospholipid membranes. The behavior of the ADE model tends toward that of the SC model for $\alpha < 1$ and toward the BC model for $\alpha > 1$.

The parameters in the ADE model are often reduced to dimensionless (or "reduced") quantities using a length scale R_a, which is defined by the average radius of a spherical vesicle with surface area A (Wortis et al., 1997), given by

$$R_a = \left(\frac{A}{4\pi}\right)^{1/2}. \tag{13}$$

The reduced spontaneous curvature is $c_0 = R_a C_0$, the reduced volume is $\nu = 3V/4\pi R_a^3$, and the reduced relaxed area difference is $\Delta a_0 = \Delta A_0/8\pi R_a D$. For spherical vesicles, $\nu = 1$ and $\Delta a_0 = 1$. The two parameters c_0 and Δa_0 can be combined to give a single parameter $\Delta\hat{a}_0 = \Delta a_0 + c_0/2\pi\alpha$, referred to as the effective reduced relaxed area difference. Because the lipid bilayer is an incompressible fluid, the average area of the vesicles, A, is expected to remain fixed at constant temperature and pH. Over the times scale of our experiments, we expect no exchange of lipids between the inner and outer leaflets of the vesicles (Wimley and Thompson, 1990), so $\Delta\hat{a}_0$ will remain constant. ΔA does, however, change during osmotic upshifts and has a significant effect on the determination of the minimum energy vesicle shape.

The volume, V, enclosed by the vesicles is constrained by the osmotic pressure. An increase to the osmolyte concentration of the external medium will induce a hyper-osmotic pressure gradient across the membrane and will result in the loss of lumenal water and a consequent reduction in vesicle volume (White et al., 1996). Using the ADE model, it is then possible to determine the minimum energy shape of a vesicle as a function of the reduced volume, ν.

Measurement of vesicle shape changes

The interpretation of experimental data in terms of the ADE phase diagram requires a priori knowledge of several parameters: the shape state of the vesicles prior to dilution, the spontaneous curvature c_0, the relaxed area difference Δa_0, and α. As will be shown in the next section, we have carefully characterized the shape state of the vesicles prior to dilution. We also use a single phospholipid species in the preparation of vesicles, which limits the value of the spontaneous curvature to 0, because membrane asymmetry is required for nonzero spontaneous curvature (Wortis et al., 1997). We expect that the relaxed area difference Δa_0 will be close to 1, because we have prepared nearly spherical vesicles. The ADE phase diagram is generic for values of α typical for phospholipids (Wortis et al., 1997), and the phase diagram calculated for $\alpha = 1.4$ (Jarić, 1995) is assumed to apply to the DOPC vesicles in this study. Vesicle shapes are determined by a comparison of the relative change in hydrodynamic radius R_h/R_a at a defined reduced volume ν, to those predicted for various axisymmetric shapes. This method of shape determination is only applicable to the case of osmotically induced shape changes because the method presupposes that the initial vesicle state is spherical and that the average surface area A does not change.

The initial hydrodynamic radius sets R_a (because the initial vesicle state is nearly spherical) and can be used to calculate the vesicle surface area, A. The reduced volume ν is determined by the imposed osmotic gradient and can be defined as

$$\nu = V/V_0 = M_{ext}/M_{int}, \tag{14}$$

where V is the enclosed volume, V_0 is the initial volume, and the osmolalities of the vesicle lumen and dilution medium (prior to equilibration) are M_{int} and M_{ext}, respectively. Changes in R_h can be compared to those calculated (as in Beney et al., 1998, outlined in Appendix A) for the axisymmetric shapes that appear in the ADE phase diagram as a function of reduced volume at constant surface area. Changes to R_h are plotted relative to R_a in Fig. 1. Although unphysical, predicted changes in R_h for vesicles where volume changes are due to changes in surface area rather than shape are also shown. We would expect, based on our estimates of c_0 and Δa_0, to measure a trajectory similar to the one shown in Fig. 1.

Assessment of vesicle elongation

As discussed previously, an essential part of this study is the preparation of a well-defined initial vesicle state to travel along a precise trajectory through the phase diagram. There have been many studies of the size and polydispersity of vesicles prepared by extrusion (Hallett et al., 1991a, b; Ertel et al., 1993; Kölchens et al., 1993; Hunter and Frisken, 1998; Korgel et al., 1998; Jin et al., 1999; Frisken et al.,

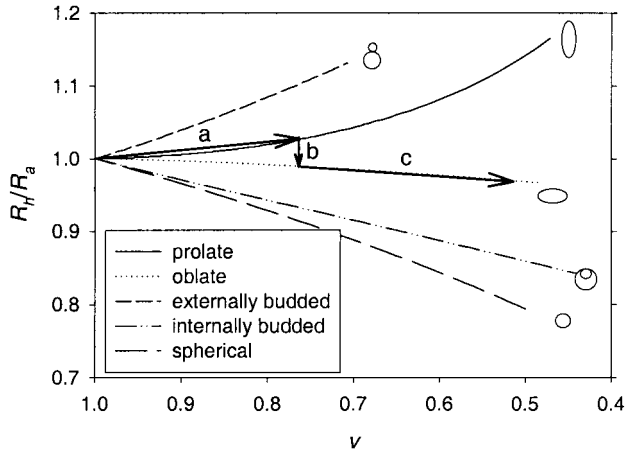

FIGURE 1 Predicted changes of the relative hydrodynamic radii R_h/R_a plotted for several vesicle shapes as a function of reduced volume v. Specific vesicle shapes have been drawn next to the corresponding curves, with their symmetry axes in the vertical direction. Also shown is an estimate of the trajectory through the ADE phase diagram corresponding to $\Delta\hat{a}_0 = 1$. *Line a*, the region of stability of prolate shapes; *b*, the prolate–oblate transition; and *c*, the region of stability of oblate shapes.

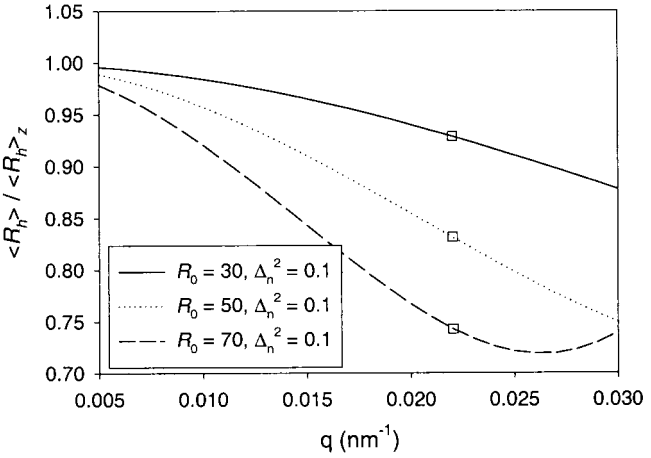

FIGURE 2 Plots of theoretical calculations of the average hydrodynamics radius as measured by cumulants analysis relative to the true z average value as a function of scattering vector q. Vesicle number distributions are represented using the log normal distribution. Three curves are shown corresponding to vesicles with log normal size distributions, varying in size with $R_0 = 30$, 50, and 70 nm. The number average polydispersity (relative variance), Δ_n^2, in each case is set to 0.1. The values for hydrodynamic radius that would be determined at a scattering angle of 90° are indicated by the open squares.

2000). Results of several of these studies demonstrate that vesicle size and polydispersity decrease as a function of increasing number of extrusions (Hunter and Frisken, 1998; Frisken et al., 2000). However, little is known about the effects of multiple extrusions on vesicle morphology.

It has been demonstrated previously (Jin et al., 1999) that, for the case of spherical or prolate vesicles, vesicle elongation can be determined quantitatively by simultaneous measurement of $\langle R_g \rangle$, $\langle R_h \rangle$, and Δ^2 by SLS and DLS. The elongation ratio of prolate vesicles has been shown to a good approximation to be

$$p^{-1} \cong 1 + 9.3\sqrt{\frac{\rho_e - 1}{-\ln(\rho_e - 1)}}, \tag{15}$$

where p^{-1} is the elongation ratio, and ρ_e is given by

$$\rho_e \cong \frac{\langle R \rangle_g + t/2}{\langle R \rangle_h}\left[1 - \frac{3}{2}\Delta_z^2 + 1.9\Delta_z^4\right], \tag{16}$$

where, following the notation of Jin et al. (1999),

$$\langle R \rangle_g \equiv \langle R_g^2 \rangle_z^{1/2}, \tag{17}$$

which is equal to $\langle R_g \rangle$, given by Eq. 8,

$$\langle R \rangle_h \equiv \frac{kT}{6\pi\eta}\langle D_T \rangle_z^{-1} = \left(\int_0^\infty R_h^{-1} m_{Rh}^2 G(R_h)\, dR_h\right)^{-1}\left(\int_0^\infty m_{Rh}^2 G(R_h)\, dR_h\right) \tag{18}$$

and

$$\Delta_z^2 = \frac{\left(\int_0^\infty R_h^{-2} m_{Rh}^2 G(R_h)\, dR_h\right)^{-1}\left(\int_0^\infty m_{Rh}^2 G(R_h)\, dR_h\right) - \langle R \rangle_h^2}{\langle R \rangle_h^2}. \tag{19}$$

It is important to note that the hydrodynamic radius and polydispersity required for the evaluation of the elongation ratio appearing in Eqs. 15 and 16 are the z (mass squared) averages. As we have discussed in the Materials and Methods section, the measured values of $\langle R_h \rangle$ and Δ^2 will only correspond to the z average quantities for small vesicles or small values of q. Figure 2 shows calculated values for $\langle R_h \rangle$ obtained by cumulants analysis for polydisperse spherical vesicles, with $\Delta_n^2 = 0.1$, as a function of scattering vector q, compared to the true z average quantities (where Δ_n^2 is the number weighted relative variance). For calculations, we use the log normal distribution to represent the vesicle size distribution, given by (Jin 1999)

$$G(R) = \frac{\exp(-\delta^2/2)}{\sqrt{2\pi}R_0\delta}\exp\left\{-\frac{\ln(R/R_0)}{2\delta^2}\right\}, \tag{20}$$

where R_0 is the peak value and δ^2 is related to the relative variance Δ^2 by $\delta^2 = \ln(1 + \Delta^2)$. It is clear that $\langle R_h \rangle$, determined from cumulants analysis, deviates substantially from the z average value for nonzero values of q. We have

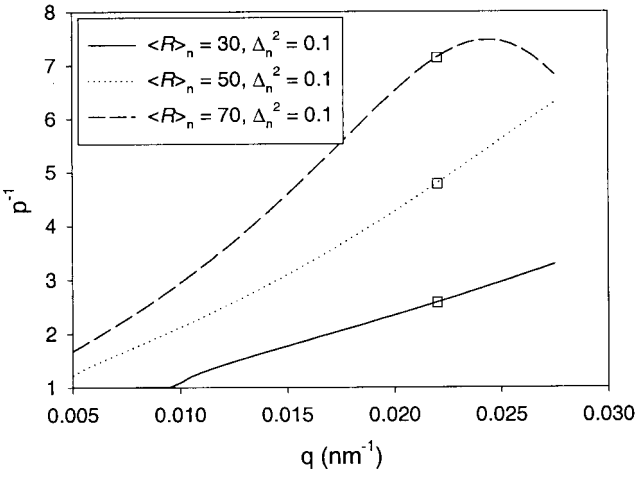

FIGURE 3 Plots of theoretical calculations of the apparent elongation ratio, p^{-1} (as given by Eqs. 15 and 16) as a function of scattering vector q. Calculations are based on results shown in Fig. 2 used with corresponding values for $\langle R_g \rangle_z$ calculated using Eq. 8. The values for elongation ratio that would be determined using DLS measurements taken at a scattering angle of 90° are indicated by the open squares.

also found similar results using the Gamma distribution (Hallett et al., 1991b) and the Weibull distribution (Korgel et al., 1998).

Deviations of both $\langle R_h \rangle$ and Δ^2 from their true z average values arise from effects of $P(q)$ and can lead to significant miscalculation of the elongation ratio as determined by Eqs. 15 and 16. In Fig. 3, we plot the apparent elongation ratio as a function of q using values for $\langle R_h \rangle$ and Δ^2 and $\langle R_g \rangle$ calculated for polydisperse spherical vesicles using Eqs. 4, 5, and 8. We find that, for nonzero values of q, the apparent value of the elongation ratio is actually significantly larger than the correct value, which is 1 for spherical, polydisperse vesicles. Consequently, Eqs. 15 and 16 are appropriate for the determination of the elongation ratio of vesicles only where $P(q)$ does not affect the measured values $\langle R_h \rangle$ and Δ^2, i.e., either when the vesicles are small or q is small. However, DLS experiments are normally performed at a scattering angle of 90°, for which the corresponding q is indicated in Figs. 2 and 3.

In this study, vesicle elongation is determined using a modification of the approach of Jin et al. (1999). Rather than use cumulant analysis to measure $\langle R_h \rangle$ and Δ^2, we perform a full inversion of the autocorrelation function to determine the intensity-weighted distribution of vesicle hydrodynamic radii $G'(R_h)$. The weightings in this distribution are a convolution of three terms, the relative number, the square of the mass, and the form factor of vesicles with hydrodynamic radius, R_h. To determine the true z average values of R_h and Δ^2, the vesicle form factors, $P(q, R_h)$, must be corrected for in the relative weightings of the distribution $G(R_h)$. Because we do not know a priori the vesicle shape, DLS measurements alone are insufficient to determine the true z average values of R_h and Δ^2. However, it is possible to use DLS and SLS data together. For simplicity, we follow Jin et al.'s (1999) assumption that a collection of vesicles will have a fixed axial ratio and have a distribution only in their mass. This assumption leads to a set of possible corrections to the measured intensity distribution $G'(R_h)$, which are described in detail in Appendix B. To determine the elongation ratio of a particular sample, we compare SLS data to theoretical data generated from DLS measurements. We use the intensity-weighted size distribution $G'(R_h)$ determined by DLS to calculate a set of hypothetical number distributions of equivalent radius, R_a (given by Eq. 13). The number distributions $G(R_a)$ each correspond to a set of vesicles with a fixed value of axial ratio, and the determination of possible solutions to $G(R_a)$ is described in detail in Appendix B. The number distributions $G(R_a)$ are then used with the appropriate form factors, given by Eqs. 9 and 11, to generate theoretical SLS curves for a series of values of axial ratios. The best agreement between the predicted and measured SLS results indicates the correct value for the axial ratio.

RESULTS AND DISCUSSION

Qualitative assessment of effects of extrusion on shape and polydispersity

The effect of increasing extrusion steps on measured values of $\langle R_g \rangle$, $\langle R_h \rangle$, and Δ^2 has been qualitatively characterized. In the case of polydisperse spherical vesicles, there will be a difference between $\langle R_g \rangle$ (corrected for membrane thickness, t) and $\langle R_h \rangle$ due to the difference in the relative weightings of vesicle sizes in the experimentally measured quantities (as given by Eqs. 4, 5, and 8). This difference will decrease as the polydispersity decreases. For prolate vesicles, the difference between $\langle R_g \rangle$ and $\langle R_h \rangle$ depends on the vesicle ellipticity, increasing with increasing ellipticity (Jin et al., 1999). In general, a separation of effects of size polydispersity and vesicle shape is nontrivial. It is, therefore, essential to use vesicles that are as monodisperse as possible. The goal is to produce vesicles for which $(\langle R_g \rangle + t/2)/\langle R_h \rangle$ is as close to 1 as possible, indicating low-polydispersity, nearly spherical vesicles.

Guinier plots of SLS measurements for DOPC vesicles extruded in sucrose buffer using a series of extrusion steps as described in the Materials and Methods section are shown in Fig. 4. Cumulants analysis of DLS measurements and Guinier analysis of SLS measurements are also summarized in Table 1. Increasing numbers of extrusion steps resulted in progressively smaller values for both $\langle R_g \rangle$ and $\langle R_h \rangle$. The difference between $\langle R_g \rangle$ and $\langle R_h \rangle$ also decreased with increasing extrusion steps. Extrusion steps were increased until a value for $(\langle R_g \rangle + t/2)/\langle R_h \rangle$ close to 1 was achieved.

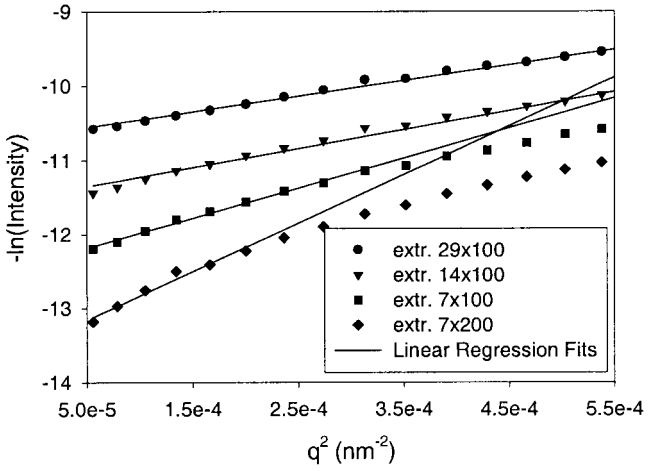

FIGURE 4 Guinier plots of SLS data measured using vesicles in isotonic sucrose. Each curve (in ascending order from bottom to top) corresponds to a successively larger number of extrusion steps as described in the Materials and Methods section. Also shown are fits using the small-angle Guinier approximation.

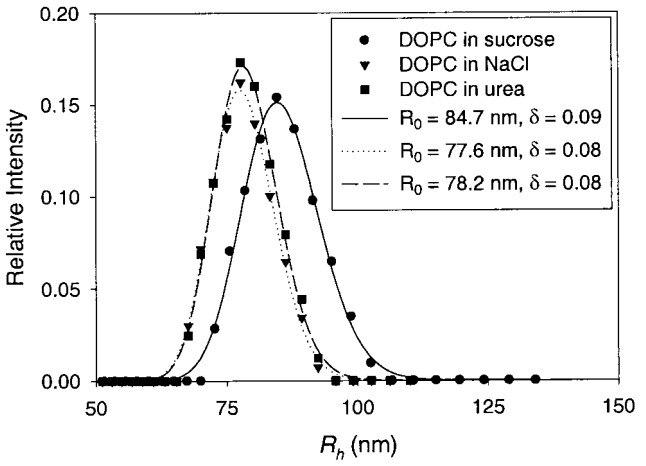

FIGURE 5 The intensity-weighted distributions in hydrodynamic radius plotted for DOPC vesicles in 100 mM NaCl, 50 mM sucrose, and 100 mM urea. Each distribution shown is the average of three distributions determined from three corresponding sets of 2-h DLS measurements. Also shown are fits to the distributions using the log normal distribution given by Eq. 20.

Measurement of vesicle size, polydispersity, and shape

Vesicles used in the hyper-osmotic upshift were further characterized by comparing SLS and DLS data as discussed in the Theory section. A reliable determination of the vesicle size distribution or polydispersity information from DLS data often requires many hours of data collection, as opposed to only a few minutes for the determination of the average radius (Kojro, 1990; Ertel et al., 1993). DLS measurements were performed on vesicles prepared in 0.1 M NaCl, 0.05 M sucrose, or 0.1 M urea under isotonic conditions. We performed DLS measurements over the course of approximately 30 h and saw no change in the size or polydispersity during this period. Intensity distributions for each sample are shown in Figure 5. Also shown are fits to the intensity distributions using the log normal distribution.

For both samples, a series of number distributions with varying axial ratio were calculated as outlined in the Theory section. These distributions were then used to generate theoretical SLS curves, which were plotted against measured SLS data as shown in Figs. 6, 7, and 8. We find, based on our comparison of simulated and measured SLS data, that DOPC vesicles extruded in NaCl, sucrose, or urea have an axial ratio close to 1. The corresponding number distributions are plotted in Fig. 9. These number distributions are used to calculate the number-averaged radius, z-averaged radius, polydispersity, and z-average radius of gyration for all three samples, shown in Table 2.

Measurement of shape changes using DLS

The primary purpose of this study was to determine the effects of osmotically induced volume reductions on the shape of LUVs using DLS. In particular, we investigated effects of hyper-osmotic dilutions on R_h of DOPC vesicles using two-membrane impermeant osmolytes, NaCl and sucrose (Paula et al., 1996, 1998) and one-membrane permeant osmolyte, urea (Paula et al., 1996) as a control. Shape changes were expected to be induced by hyper-osmotic dilution of vesicles in the membrane-impermeant solutes, NaCl and sucrose, whereas no changes were expected for dilutions in the membrane-permeant solute, urea. For each sample, DLS measurements were performed immediately after dilution and again after 12 h to verify that there was no time dependence in the measured hydrodynamic radii that could result from slow relaxation due to solute leakage or

TABLE 1 Effects of extrusion passes on apparent $(\langle R_g\rangle + t/2)/\langle R_h\rangle$ for DOPC vesicles extruded in sucrose

Extrusion Passes	$\langle R_g\rangle$ (nm)	$\langle R_h\rangle$ (nm)	$(\langle R_g\rangle + t/2)/\langle R_h\rangle$
7 × 200 nm	140.2	98.2	1.44
7 × 200 nm + 7 × 100 nm	100.2	84.6	1.20
7 × 200 nm + 14 × 100 nm	87.4	76.6	1.16
7 × 200 nm + 29 × 100 nm	82.8 ± 1.6	73.84 ± 0.28	1.14 ± 0.03

Details concerning the method of extrusion are given in the Materials and Methods section.

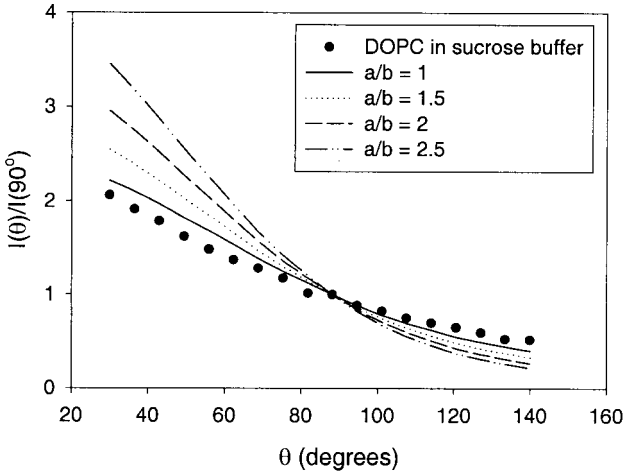

FIGURE 6 Plots of theoretical SLS intensity curves calculated using number distributions calculated using a range of axial ratios (as described in the Theory section) from DLS for DOPC vesicles prepared in sucrose buffer. Also shown is actual SLS data for the same sample. Data is shown normalized to the scattered intensity at 90°.

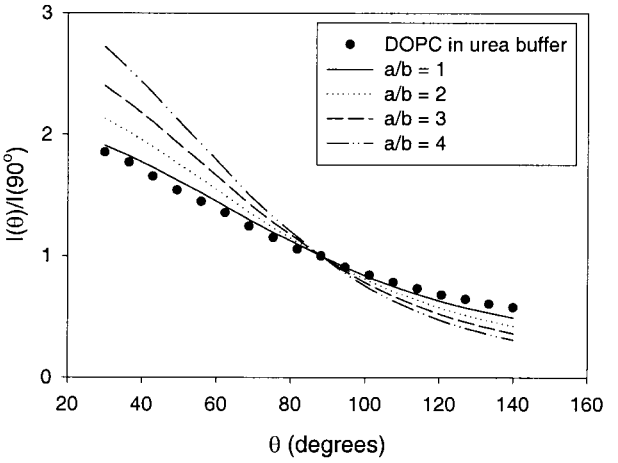

FIGURE 8 Plots of theoretical SLS intensity curves calculated using number distributions calculated using a range of axial ratios (as described in the Theory section) from DLS for DOPC vesicles prepared in urea buffer. Also shown is experimental SLS data for the same sample. Data is shown normalized to the scattered intensity at 90°.

lipid flip-flop. In this case, measurements are an average of at least 10 runs of 5 min each.

Figure 10 shows results of DLS measurements on DOPC vesicles exposed to hyper-osmotic solutions of urea. As expected, there is no change in the measured hydrodynamic radius either immediately after dilution or after the samples have been allowed to sit for ~12 h. Figure 11 shows DLS results for DOPC in hyper-osmotic solutions of NaCl measured immediately after dilution and again after 12 h. In this case, we see that the measured hydrodynamic radius gradually decreases with decreasing ν and follows the behavior expected for oblate vesicles. For each hyper-osmotic shift, the hydrodynamic radii show no change between the initial and final measurement. Also shown in Figure 11 are similar results for DOPC vesicles in sucrose. In sucrose, the DOPC vesicles also appear to become oblate over the full range of volume reductions and also show no change after a period of 12 h.

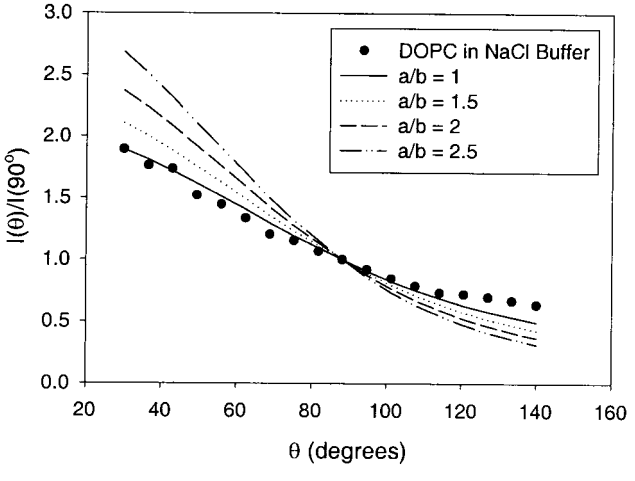

FIGURE 7 Plots of theoretical SLS intensity curves calculated using number distributions calculated using a range of axial ratios (as described in the Theory section) from DLS for DOPC vesicles prepared in NaCl buffer. Also shown is experimental SLS data for the same sample. Data is shown normalized to the scattered intensity at 90°.

Comparison of the measured shape trajectory with predictions of the ADE model

The ADE model predicts that, for $c_0 = 0$, $\Delta a_0 = 1$, and $\alpha = 1.4$, vesicles should first become prolate for $\nu > 0.75$ then

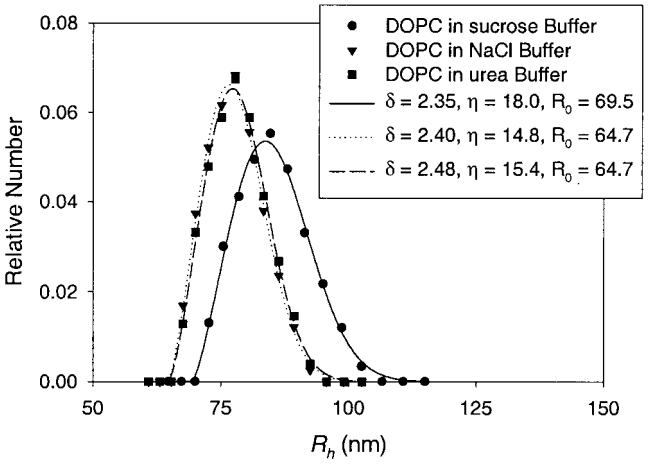

FIGURE 9 Plots of number distributions of hydrodynamic radii for vesicles prepared in sucrose, NaCl, or urea buffer. Also shown are fits to the distributions using the Weibull distribution, as described in Korgel et al. (1998).

TABLE 2 Number $\langle R_h \rangle_n$ and Z average $\langle R_h \rangle_z$ hydrodynamic radii, number average polydispersity Δ_n^2, and radius of gyration $\langle R_g \rangle^*$, calculated from number distributions shown in Fig. 9

Buffer	$\langle R_h \rangle_n$ (nm)	$\langle R_h \rangle_z$ (nm)	Δ_n^2	$\langle R_g \rangle^*$ (nm)	$\langle R_s \rangle^*$ (nm)
Sucrose	85.5	88.0	0.007	86.4	84.2
NaCl	77.8	79.7	0.006	77.9	75.4
Urea	78.4	80.2	0.006	78.5	78.2

Also shown are values for the radius of gyration $\langle R_g \rangle^+$ determined from SLS measurements.

oblate for $\nu < 0.75$ (Jarić et al., 1995). However, the measurements indicate that DOPC vesicles exposed to hyper-osmotic stress are oblate over the full range of volume reductions. These results bring into question the accuracy of the estimates of c_0 and Δa_0 and the assumed value of α. Therefore, before any conclusions are made concerning the possible disagreement between the predictions of the ADE model and our results, it is necessary to examine the possible effects of varying c_0, Δa_0, and α.

As discussed earlier, we have assumed that $c_0 = 0$ because we are dealing with a single lipid system. It has recently been demonstrated that preferential solute interactions or solute asymmetry can induce a change in spontaneous curvature (Döbereiner et al., 1999). It is possible that a solute gradient across the membrane could have the effect of producing a nonzero spontaneous curvature, if the solute were to preferentially associate with the membrane rather than being excluded from the surface. However, measurements using two very different solutes, NaCl, an ionic solute, and sucrose, a sugar, produced identical results. This leaves little reason to believe

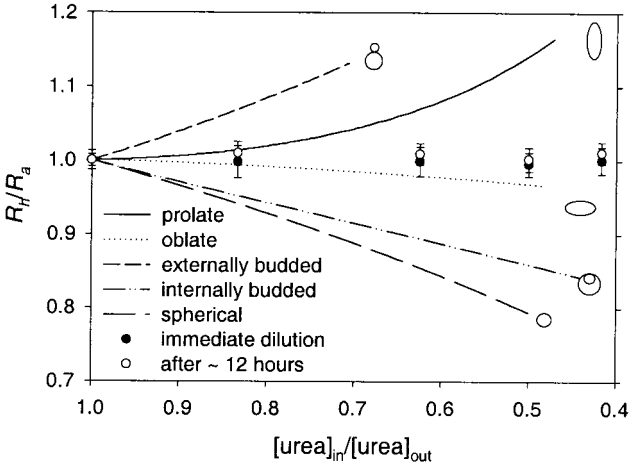

FIGURE 10 Hydrodynamic radii of vesicles extruded in 100 mM urea and diluted hyper-osmotically into urea, plotted versus the ratio of the initial internal and external urea concentrations, $[urea]_{in}/[urea]_{out}$. Data are plotted for vesicles immediately after dilution and approximately 12 h after dilution. Also plotted are curves showing predicted changes to hydrodynamic radii for several axisymmetric shapes, assuming a reduced volume equal to the ratio of the initial internal and external urea concentrations, $[urea]_{in}/[urea]_{out}$.

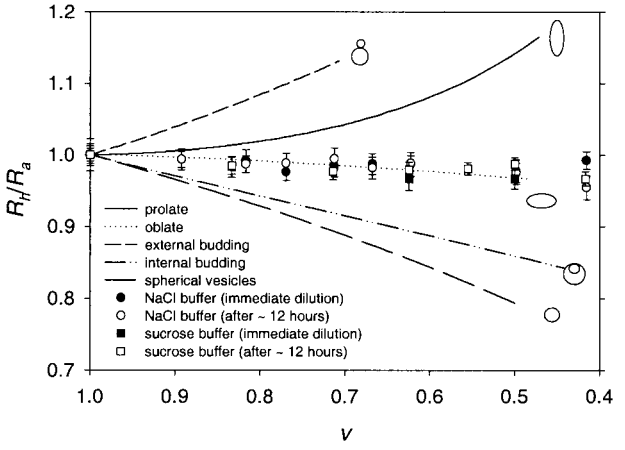

FIGURE 11 Changes to hydrodynamic radii of DOPC vesicles prepared in 100 mM NaCl (*circles*) or 50 mM sucrose (*squares*) due to hyper-osmotic upshifts in NaCl. Data are plotted for vesicles immediately after dilution (*closed symbols*) and ~12 h after dilution (*open symbols*). Also plotted are curves showing predicted changes to hydrodynamic radii for several axisymmetric shapes.

that our observations could be the result of a solute-induced change to the spontaneous curvature.

There is some evidence that vesicles prepared by extrusion can have a distribution of relaxed area differences Δa_0, rather than all vesicles achieving the equilibrium value (Mui et al., 1995). Such a distribution would be expected to result in a distribution of shapes upon hyper-osmotic shift with a corresponding average hydrodynamic radius intermediate between those predicted for single shapes. The value of the observed R_h would depend on the relative abundance of each shape state at a particular reduced volume. Because the measured hydrodynamic radii lie on the oblate line for all volume reductions, the presence of any other shapes is likely to be insignificant. Thus we conclude that the area difference Δa_0 is likely to be nearly uniform.

The final parameter to be considered is α, the ratio of the nonlocal k_c to local k_t bending moduli. Although the features of the ADE phase diagram (such as phase boundaries) are generic for all values of α (Wortis et al., 1997), their positions in the phase diagram will depend on the particular value of α. The ADE phase diagram to which we have referred has been calculated for $\alpha = 1.4$, because this was the original estimate for SOPC (Miao et al., 1994). How-

TABLE 3 Experimental measurements of the elastic and stretching moduli of SOPC and DOPC and corresponding estimates of α

Lipid	k_c (10^{-19} J)	K (mN/m)	D (nm)	α
SOPC*	0.90 ± 0.06	200 ± 13	28.5 ± 1.5	1.4
DOPC†	0.85 ± 0.10	265 ± 18	26.9 ± −0.4	1.8

*Miao 1994.
†Rawicz 2000.

ever, there have been more recent measurements of the nonlocal bending modulus k_c, the area compressibility K, and bilayer mechanical thickness D (Rawicz et al., 2000) which can be used to estimate α from the relation $\alpha = KD^2/4\pi k_c$ (Miao et al., 1994). Table 3 summarizes the results of these measurements and corresponding estimates of α for SOPC and DOPC. Our estimate of α from this data, $\alpha_{DOPC} = 1.8$, is somewhat larger than the value 1.4 used to construct the ADE phase diagram. An increase in α results in a shift of the ADE phase diagram toward behavior characteristic of the BC model, which predicts only oblate vesicles under the conditions of our experiments (Seifert et al., 1991). We can speculate that an increase in α would cause a shift of the prolate–oblate transition (Fig. 1, *line B*) to higher values of ν. For sufficiently large values of α, the prolate–oblate transition should effectively vanish. Because we cannot distinguish between prolate and oblate vesicles for ν larger than 0.9, it is possible that the prolate–oblate transition has either shifted out of the range of sensitivity of our measurements or has disappeared altogether.

CONCLUSIONS

In this study, low polydispersity vesicles were needed to investigate effects of hyper-osmotic stress on vesicle shape. By performing a large number of extrusion steps, it was possible to produce vesicles that were nearly spherical and had a very narrow size distribution (as shown in Fig. 9). Vesicle shape changes were measured as a function of reduced volume by comparing relative changes to the hydrodynamic radius with those predicted for several axisymmetric shapes as a function of reduced volume with constant surface area A. We found very close agreement between our results and the predicted changes to relative hydrodynamic radii corresponding to oblate vesicles.

As part of this study, our results were compared with predictions of the ADE model. A necessary part of this comparison required that we make certain assumptions about properties of our vesicles, that $\alpha \sim 1.4$, $\Delta a_0 = 1$, and $c_0 = 0$. For estimated values of α, Δa_0, and c_0, the ADE model predicts that prolate shapes should appear in the region $\nu > 0.75$ and oblate shapes should appear for $\nu < 0.75$. However, only oblate shapes were observed for all imposed changes to the reduced volume. Although there are several possible explanations for the apparent discrepancy between these results and the predictions of the ADE model, we propose that it is a consequence of the difference in values of α between DOPC ($\alpha = 1.8$) and that used to construct the phase diagram ($\alpha = 1.4$).

Dynamic light scattering has been demonstrated to be an effective technique for studying shape changes in LUVs. However, more work is required in determining the effects of changes in α on the ADE phase diagram, and the effects of a variation in lipid composition on shape changes. Currently, we are performing measurements on a variety of lipid species expected to span a range of values of α; this should allow a better test of the ADE model, because a variation in α should produce a variation in measured shape behavior of hyper-osmotically stressed vesicles.

APPENDIX A

Calculation of vesicle hydrodynamic radii as a function of reduced volume depends on several assumptions: that the vesicles are spherical prior to exposure to an osmotic gradient, that the surface area of the membrane remains constant, and that the vesicles act as ideal osmometers (i.e., the final volume enclosed by the vesicles is determined by the imposed osmotic gradient. The hydrodynamic radii for four possible vesicle shapes: prolate ellipsoids, oblate ellipsoids, externally budded vesicles, and internally budded vesicles, have been calculated as follows.

Ellipsoids

Calculation of the hydrodynamic radii for prolate and oblate ellipsoids follows that of Beney et al. (1998). For both prolate and oblate vesicles, we define the symmetry axis as a and the perpendicular axis as b. In this notation, for prolate vesicles, a is the semimajor axis and b is the semiminor axis, and for oblate vesicles, a is the semiminor axis and b is the semimajor axis. The corresponding eccentricity parameters are defined as

$$e_{pro} = \left(1 - \frac{b^2}{a^2}\right)^{1/2}, \tag{A1}$$

$$e_{obl} = \left(1 - \frac{a^2}{b^2}\right)^{1/2}, \tag{A2}$$

for prolate and oblate vesicles, respectively. For both cases, an eccentricity of 0 corresponds to spherical vesicles. The hydrodynamic radius for a prolate vesicle is given by (Berne and Pecora, 2000)

$$R_{hpro} = \left[\frac{1}{ae_{pro}} \ln \frac{a(1 + e_{pro})}{b}\right]^{-1}. \tag{A3}$$

The corresponding volume and surface area are given by (Beney et al., 1998)

$$V_{pro} = \tfrac{4}{3}\pi ab^2, \tag{A4}$$

$$A_{pro} = 2\pi\left(b^2 + \frac{ab}{e_{pro}} \sin^{-1} e_{pro}\right). \tag{A5}$$

The hydrodynamic radius for oblate vesicles is given by (Berne and Pecora, 2000)

$$R_{hobl} = \left[\frac{1}{be_{obl}} \tan^{-1} \frac{be_{obl}}{a}\right]^{-1}. \tag{A6}$$

The corresponding volume and surface area for oblate vesicles are given by (Beney et al., 1998)

$$V_{obl} = \tfrac{4}{3}\pi ab^2 \tag{A7}$$

$$A_{obl} = 2\pi\left(b^2 + \frac{a^2}{2e_{obl}} \ln \frac{1 + e_{obl}}{1 - e_{obl}}\right). \tag{A8}$$

To determine the relationship between vesicle hydrodynamic radius and reduced volume, we calculate both quantities over a range of ellipticities. Because there exists the constraint of constant surface area, the semimajor

axes of the prolate and oblate ellipsoids can be defined in terms of the corresponding ellipticity parameters, e_{pro} and e_{obl}, and area, A:

$$a_{pro} = A^{1/2}\left[2\pi\left\{(1 - e_{pro}^2) + \frac{\sqrt{1 - e_{pro}^2}}{e_{pro}}\sin^{-1}e_{pro}\right\}\right]^{-1/2}, \quad \text{(A9)}$$

$$b_{obl} = A^{1/2}\left[2\pi\left\{1 + \left(\frac{1 - e_{obl}^2}{2e_{obl}}\right)\ln\left(\frac{1 + e_{obl}}{1 - e_{obl}}\right)\right\}\right]^{-1/2}. \quad \text{(A10)}$$

The relationship between the hydrodynamic radii and corresponding vesicle volumes can be determined by calculating R_h and the corresponding V over a range of ellipticities. Results for prolate and oblate vesicles are plotted in Fig. 1.

Externally budded vesicles

For externally budded vesicles, the effective hydrodynamic radius can be calculated as a collection of n attached, arbitrarily sized beads, given by (Richards, 1980)

$$R_h = \frac{\left(\sum_{i=1}^{n} b_i^2\right)^2}{\sum_{i=1}^{n} b_i^3 + \sum_{i=1}^{n}\sum_{j=1,i\neq j}^{n} b_i^2 b_j^2 r_{ij}^{-1}}, \quad \text{(A11)}$$

where n is the total number of beads, b_i is the radius of bead i, and r_{ij} is the distance between the centers of beads i and j. We will restrict our consideration to a vesicle with one external bud. In this case, Eq. A11 simplifies to

$$R_h = \frac{(r_1^2 + r_2^2)^2}{r_1^3 + r_2^3 + 2r_1^2 r_2^2 (r_1 + r_2)^{-1}}, \quad \text{(A12)}$$

where r_1 is the radius of the parent vesicle and r_2 is the radius of the budded vesicle, so that, in the case of a spherical vesicle with radius r_0, $r_1 = r_0$, $r_2 = 0$, and $R_h = r_0$. In this calculation, we assume that the neck attaching both vesicles is small. The constraint of constant surface area defines the relationship between r_1 and r_2, given by

$$r_2 = \sqrt{r_0^2 - r_1^2}. \quad \text{(A13)}$$

The corresponding volume of the externally budded vesicle can be expressed in terms of r_1 and r_0 as

$$v_{ext} = \tfrac{4}{3}\pi[r_1^3 + (r_0^2 - r_1^2)^{3/2}]. \quad \text{(A14)}$$

We can then determine the relationship between the hydrodynamic radii and corresponding vesicle volumes by calculating R_h and the corresponding V over a range of r_1. The hydrodynamic radii of externally budded vesicles as a function of reduced volume are plotted in Fig. 1.

Internally budded vesicles

For the case of internally budded vesicles, it is assumed that the hydrodynamic radius will correspond to that of the external vesicle and that the neck between the two vesicles is small. In this case, the restriction of constant surface area relates the smaller vesicle radius and larger vesicle radius in the same way as for externally budded vesicles,

$$R_h = r_2 = \sqrt{r_0^2 - r_1^2}. \quad \text{(A15)}$$

In this case, however, the reduced volume is defined by the difference between the larger and smaller vesicle volumes and is given by

$$v_{int} = \tfrac{4}{3}\pi[r_1^3 - (r_0^2 - r_1^2)^{3/2}]. \quad \text{(A16)}$$

Again, we can then determine the relationship between the hydrodynamic radii and corresponding vesicle volumes by calculating R_h and the corresponding V over a range of r_1. The hydrodynamic radii of internally budded vesicles as a function of reduced volume are also plotted in Fig. 1.

APPENDIX B

As discussed earlier, an essential part of this study is the characterization of the state of extruded vesicles prior to hyper-osmotic dilution. To determine vesicle number distributions from the measured intensity distribution, following the work of Jin et al. (1999), it is assumed that, although vesicles are polydisperse, every vesicle in the system will have the same axial ratio. This assumption allows us to correct for effects of ellipticity in both the apparent hydrodynamic radius and relative weighting of each size given by the intensity distribution.

For the purposes of computation, it is convenient to redefine the intensity-weighted size distribution in terms of the equivalent radius, R_a (given by Eq. 13), rather than the hydrodynamic radius R_h. From Eqs. A5 and A9, we find that, for fixed axial ratios, R_a is related to R_h by

$$R_a = \frac{R_h}{\sqrt{2}e_{pro}}\left[(1 - e_{pro}^2) + \frac{\sqrt{1 - e_{pro}^2}}{e_{pro}}\sin^{-1}(e_{pro})\right]^{1/2} \times \ln\left(\frac{1 + e_{pro}}{\sqrt{1 - e_{pro}^2}}\right). \quad \text{(B1)}$$

Using this equation, we can then redefine the intensity-weighted size distribution in terms of the equivalent radius R_a. For each value of R_a, we calculate the vesicle surface area A, which is proportional to its mass. Using the area A, the ellipticity e_{pro}, and Eqs. A1 and A9, it is possible to determine values for the long and short axes, a and b, which are then used in Eq. 11 to determine the vesicle scattering factor $P(q, R_a, e_{pro})$. The vesicle number distributions are then calculated for specific values of axial ratio, by dividing the intensity weighting of each R_a by A^2 and $P(q, R_a, e_{pro})$.

SLS measured from polydisperse vesicles is equal to the mass-squared weighted average of the scattering factor $P(q, R_a, e_{pro})$ given by

$$\langle P(q,R_a,e_{pro})\rangle = \int_0^\infty m_{Ra}^2 P(q,R_a,e_{pro}) G(R_a)\, dR_a \times \left(\int_0^\infty m_{Ra}^2 G(R_a)\, dR_a\right)^{-1}, \quad \text{(B2)}$$

where m_{Ra} is the mass of vesicles with equivalent radius R_a, and R_a has been corrected for the vesicle thickness t, which is assumed to be 4 nm. The number distribution $G(R_a)$ is modeled using the Weibull distribution (Korgel et al., 1998) given by

$$G(R_a) = \frac{\delta}{\eta}\left|\frac{R_a - R_0}{\eta}\right|^{\delta - 1}\exp\left(-\left|\frac{R_a - R_0}{\eta}\right|^{\delta}\right). \quad \text{(B3)}$$

For each value of axial ratio a/b (or corresponding ellipticity, e_{pro}), theoretical SLS curves are calculated using the number distributions determined above and Eqs. B2 and B3.

The authors would like to thank C. Schultz-Nielsen for his work on some of the analysis software used in this study. The authors also gratefully acknowledge enlightening discussions with B. J. Frisken, and B. G. Nickel.

This research was supported by the Natural Sciences and Engineering Research Council of Canada.

REFERENCES

Agirre, A., C. Flach, F. M. Goñi, R. Mendelsohn, J. M. Valpuesta, F. Wu, and J. L. Nieva. 2000. Interactions of the HIV-1 fusion peptide with large unilamellar vesicles and monolayers. A cryo-TEM and spectroscopic study. *Biochim. Biophys. Acta.* 1467:153–164.

Bagatolli, L. A., and E. Gratton. 1999. Two-photon fluorescence microscopy observation of shape changes at the phase transition in phospholipid giant unilamellar vesicles. *Biophys. J.* 77:2090–2101.

Beney, L., E. Linares, and E. Ferret, and P. Gervais. 1998. Influence of the shape of phospholipid vesicles on the measurement of their size by photon correlation spectroscopy. *Eur. Biophys. J.* 27:567–574.

Berne, B. J., and R. Pecora. 2000. Dynamic Light Scattering. Dover Publications, Inc., New York.

Booth, P. J., M. L. Riley, S. L. Flitsch, R. H. Templer, A. Farooq, A. R. Curran, N. Chadborn, and P. Wright. 1997. Evidence that bilayer bending rigidity affects membrane protein folding. *Biochemistry.* 36: 197–203.

Brocca, P., L. Cantù, M. Corti, and E. Del Favero. 2000. Thermal fluctuations of small vesicles: observation by dynamic light scattering. *Progr. Colloid Polym. Sci.* 115:181–185.

Burack, W. R., A. R. G. Dibble, M. M. Allietta, and R. L. Biltonen. 1997. Changes in vesicle morphology induced by lateral phase separation modulate phospholipase A_2 activity. *Biochemistry.* 36: 10551–10557.

Döbereiner, H.-G., E. Evans, M. Kraus, U. Seifert, and M. Wortis. 1997. Mapping vesicle shapes into the phase diagram: a comparison of experiment and theory. *Phys. Rev. E.* 55:4458–4474.

Döbereiner, H.-G., O. Selchow, and R. Lipowsky. 1999. Spontaneous curvature of fluid vesicles induced by trans-bilayer sugar asymmetry. *Eur. Biophys. J.* 28:174–178.

Döbereiner, H.-G. 2000. Properties of giant vesicles. *Curr. Opin. Coll. Int. Sci.* 5:256–263.

Edwards, K., M. Johnsson, G. Karlsson, and M. Silvander. 1997. Effect of polyethyleneglycol-phospholipids on aggregate structure in preparations of small unilamellar liposomes. *Biophys. J.* 73:258–266.

Ertel, A., A. G. Marangoni, J. Marsh, F. R. Hallett, and J. M. Wood. 1993. Mechanical properties of vesicles. I. Coordinated analysis of osmotic swelling and lysis. *Biophys. J.* 64:426–434.

Frisken, B. J., C. Asman, and P. J. Patty. 2000. Studies of vesicle extrusion. *Langmuir.* 16:928–933.

Gregoriadis, G. 1995. Engineering liposomes for drug delivery: progress and problems. *Trends Biochnol.* 13:527–537.

Guinier, A. 1994. X-Ray Diffraction in Crystals, Imperfect Crystals and Amorphous Bodies. Dover Publications, Inc., New York.

Hallett, F. R., T. Craig, J. Marsh, and B. Nickel. 1989. Particle size analysis: number distributions by dynamic light scattering. *Can. J. Spectrosc.* 34:63–70.

Hallett, F. R., B. Nickel, C. Samuels, and P. H. Krygsman. 1991a. Determination of vesicle size distributions by freeze-fracture electron microscopy. *J. Electron Micros. Tech.* 17:459–466.

Hallett, F. R., J. Watton, and P. Krygsman. 1991b. Vesicle sizing: number distributions by dynamic light scattering. *Biophys. J.* 59:357–362.

Helfrich, W. 1973. Elastic properties of lipid bilayers: theory and possible experiments. *Z. Naturforsch.* 28:693–703.

Hunter, D. G., and B. J. Frisken. 1998. Effect of extrusion pressure and lipid properties on the size and polydispersity of lipid vesicles. *Biophys. J.* 74:2996–3002.

Jarić, M., U. Seifert, W. Wintz, and M. Wortis. 1995. Vesicular instabilities: the prolate-to-oblate transition and other shape instabilities of fluid bilayer membranes. *Phys. Rev. E.* 52:6623–6634.

Jin, A. J., D. Huster, K. Gawrisch, and R. Nossal. 1999. Light scattering characterization of extruded lipid vesicles. *Eur. Biophys. J.* 28: 187–199.

Johnson, C. S., and D. A. Gabriel. 1994. Laser Light Scattering. Dover Publications, Inc., New York.

Kölchens, S., V. Ramaswami, J. Birgenheier, L. Nett, and D. F. O'Brian. 1993. Quasi-elastic light scattering determination of the size distribution of extruded vesicles. *Chem Phys. Lipids.* 65:1–10.

Kojro, Z. 1990. Influence of statistical errors on size distributions obtained from dynamic light scattering data. Experimental limitations in size distribution determination. *J. Phys. A. Math. Gen.* 23:1363–1383.

Koppel, D. E. 1972. Analysis of macromolecular polydispersity in intensity correlation spectroscopy: the method of cumulants. *J. Chem. Phys.* 57:4814–4820.

Korgel, B. A., J. H. van Zanten, and H. G. Monbouquette. 1998. Vesicle size distributions measured by flow field-flow fractionation coupled with multiangle light scattering. *Biophys. J.* 74:3264–3272.

Lerebours, B., E. Wehrli, and H. Hauser. 1993. Thermodynamic stability and osmotic sensitivity of small unilamellar phosphatidylcholine vesicles. *Biochim. Biophys. Acta.* 1152:49–60.

MacDonald, R. C., R. I. MacDonald, B. Ph. M. Menco, K. Takeshita, N. K. Subbarao, and L.-R. Hu. 1991. Small-volume extrusion apparatus for preparation of large, unilamellar vesicles. *Biochim. Biophys. Acta.* 1061:297–303.

Miao, L., U. Seifert, M. Wortis, and H.-G. Döbereiner. 1994. Budding transitions of fluid-bilayer vesicles: the effect of area-difference elasticity. *Phys. Rev. E.* 49:5389–5407.

Mui, B. L.-S., P. R. Cullis, E. A. Evans, and T. D. Madden. 1993. Osmotic properties of large unilamellar vesicles prepared by extrusion. *Biophys. J.* 64:443–453.

Mui, B., H.-G. Döbereiner, T. D. Madden, and P. R. Cullis. 1995. Influence of transbilayer area asymmetry on the morphology of large unilamellar vesicles. *Biophys. J.* 69:930–941.

Paula, S., A. G. Volkov, A. N. Van Hoek, T. H. Haines, and D. W. Deamer. 1996. Permeation of protons, potassium ions, and small polar molecules through phospholipid bilayers as a function of membrane thickness. *Biophys. J.* 70:339–348.

Paula, S., A. G. Volkov, and D. W. Deamer. 1998. Permeation of halide anions through phospholipid bilayers occurs by the solubility-diffusion mechanism. *Biophys. J.* 74:319–327.

Rawicz, W., K. C. Olbrich, T. McIntosh, D. Needham, and E. Evans. 2000. Effect of chain length and unsaturation on elasticity of lipid bilayers. *Biophys. J.* 79:328–339.

Richards, E. G. 1980. An Introduction to Physical Properties of Large Molecules in Solution. Cambridge University Press, New York. 170–172.

Sackmann, E. 1995. Physical basis of self-organization and function of membranes: physics of vesicles. *In* Handbook of Biological Physics, Vol. 1. R. Lipowsky and E. Sackmann, editors. Elsevier Science, New York. 216–217.

Seifert, U., K. Berndl, R. Lipowsky. 1991. Shape transformations of vesicles: phase diagram for spontaneous-curvature and bilayer-coupling models. *Phys. Rev. A.* 44:1182–1202.

Svetina, S., and B. Žekš. 1983. Bilayer couple hypothesis of red cell shape transformations and osmotic hemolysis. *Biomed. Biochim. Acta.* 42: S86–S90.

Talmon, Y., J. L. Burns, M. H. Chestnut, and D. P. Siegel. 1990. Time-resolved cryotransmisson electron microscopy. *J. Electron Micros. Tech.* 14:6–12.

White, G., J. Pencer, B. G. Nickel, J. M. Wood, and F. R. Hallett. 1996. Optical changes in unilamellar vesicles experiencing osmotic stress. *Biophys. J.* 71:2701–2715.

White, G. F., K. I. Racher, A. Lipski, F. R. Hallett, and J. M. Wood. 2000. Physical properties of liposomes and proteoliposomes prepared from *Escherichia coli* polar lipids. *Biochim. Biophys. Acta.* 1468: 175–186.

Wimley, W. C., and T. E. Thompson. 1990. Exchange and flip-flop of dimyristoylphosphatidylcholine in liquid-crystalline, gel and two-component, two-phase large unilamellar vesicles. *Biochemistry.* 29: 1296–1303.

Wood, J. M. 1999. Osmosensing by bacteria: signals and membrane-based sensors. *Microbiol. Molec. Biol. Reviews.* 63:230–262.

Wortis, M., M. Jarić, and U. Seifert. 1997. Thermal shape fluctuations of fluid-phase phospholipid-bilayer membranes and vesicles. *J. Mol. Liq.* 71:195–207.

Xu, L., and H.-G. Döbereiner. 1999. Amplitude hierarchy of vesicle shapes. *J. Biol. Phys.* 25:35–39.